



# Geometry-dependent analysis of 2p3d- and 2p3s-partial fluorescence yield spectra for high-spin 3d<sup>5</sup> systems

Saki Imada<sup>a,\*</sup>, Frank M.F. de Groot<sup>b</sup>

<sup>a</sup> Faculty of Electrical Engineering and Electronics, Kyoto Institute of Technology, Kyoto 606-8585, Japan

<sup>b</sup> Debye Institute for Nanomaterials Science, Utrecht University, Utrecht 3584, the Netherlands

## ARTICLE INFO

### Keywords:

X-ray absorption spectroscopy  
 Partial fluorescence yield spectrum  
 Resonant inelastic X-ray emission spectroscopy  
 Geometry dependence  
 Propagation direction selection rule

## ABSTRACT

Geometry dependences of partial fluorescence yield (PFY) spectra at the L<sub>2,3</sub>-edge of 3d transition metals are discussed theoretically and experimentally for high-spin 3d<sup>5</sup> systems in O<sub>h</sub> and T<sub>d</sub> point symmetries. Firstly, linear polarized light's propagation direction selection rules for a two-photon process are applied to 2p3d-PFY spectroscopy. Then, the 2p3d-PFY spectra were analyzed by comparison with spectra obtained as partial integration of 2p3d-resonant inelastic X-ray scattering (RIXS) signals, utilizing the relationship between PFY and RIXS spectroscopies: the former is an integration of yield of emitted light at each excitation energy, and the latter is a dispersion of emitted light as a function of emission energy at each excitation energy. Thus, a PFY spectrum can be divided into super PFY (sPFY) spectra using partial integrations of signals on a RIXS map, such as sPFY spectra from elastic and inelastic signals. It is suggested that the origin of the large deviation of 2p3d-PFY spectral shape in a linear-horizontal geometry from a true X-ray absorption spectrum is due to the lack of elastic signals, i.e., the lack of signals emitted when the system returns to its ground state. Contrary to a 2p3d-PFY spectrum, a 2p3s-PFY spectrum is often assumed to have a one-to-one correspondence with true XAS; however, 2p3s-PFY spectroscopy is also a two-photon process that abides by the propagation direction selection rules. We will show theoretically that 2p3s-PFY spectral shapes show a geometry dependence and offer a way to obtain a true X-ray absorption structure from a combination of 2p3s-PFY spectra in linear-vertical and linear-horizontal geometries.

## 1. Introduction

X-ray absorption spectroscopy (XAS) at L<sub>2,3</sub> edges is a powerful technique to investigate the electronic structure of 3d transition metal systems [1]. There are multiple ways to acquire X-ray absorption intensities, such as transmission, electron yield (EY), and fluorescence yield (FY) detection. To investigate bulk properties of a material, a 2p3d-partial FY (2p3d-PFY) spectrum is widely used, although it has been indicated that a 2p3d-PFY differs from an X-ray absorption cross-section; the fluorescence yield depends on the specific X-ray absorption final state (2p<sup>5</sup>3d<sup>n+1</sup>), which results in a modified spectral shape from true XAS [2–4]. This state-dependency of fluorescence is an intrinsic effect that cannot be avoided in the two-photon process between 2p and 3d orbitals. Moreover, the spectral shape is dependent on the experimental geometry, for example, linear horizontal (LH) and linear vertical (LV) geometries [4–6]. If one does not include this geometry dependence, this can lead to mistakes in the 2p3d-PFY spectral

analysis.

Shifting our perspective, 2p3d-PFY spectra can give us unique information precisely because of the two-photon process, in analogy with 2p3d-resonant X-ray emission (RXE, or resonant inelastic X-ray scattering, RIXS) spectroscopy. In 2p3d-RIXS spectroscopy, 3d excited multiplet states of a transition metal surrounded by ligands are often discussed [7–12]. As the final state of 2p3d-RIXS has no core hole, the deduced multiplet structures correspond to (multi-electronic) valence-excitations, usually analyzed with the so-called Tanabe-Sugano diagram [13]. One of the interesting options of 2p3d-RIXS spectroscopy is geometry-dependent measurements with a 90-degree scattering angle. Using selection rules for the two-photon process, the incident photon's polarization dependences of the elastic peaks in the 2p3d-RIXS spectra have been discussed [14,15]. Elastic emissions result from the system returning to its ground state, while inelastic emissions are related to low-energy excited states. Thus, by analyzing the elastic and inelastic signals of 2p3d-RIXS, the 3d<sup>n</sup> multiplet structure can be determined in

\* Corresponding author.

E-mail addresses: [saki\\_imada@kit.ac.jp](mailto:saki_imada@kit.ac.jp) (S. Imada), [F.M.F.deGroot@uu.nl](mailto:F.M.F.deGroot@uu.nl) (F.M.F. de Groot).

<https://doi.org/10.1016/j.elspec.2025.147538>

Received 27 November 2024; Received in revised form 14 March 2025; Accepted 25 March 2025

0368-2048/© 2025 Elsevier B.V. All rights are reserved, including those for text and data mining, AI training, and similar technologies.

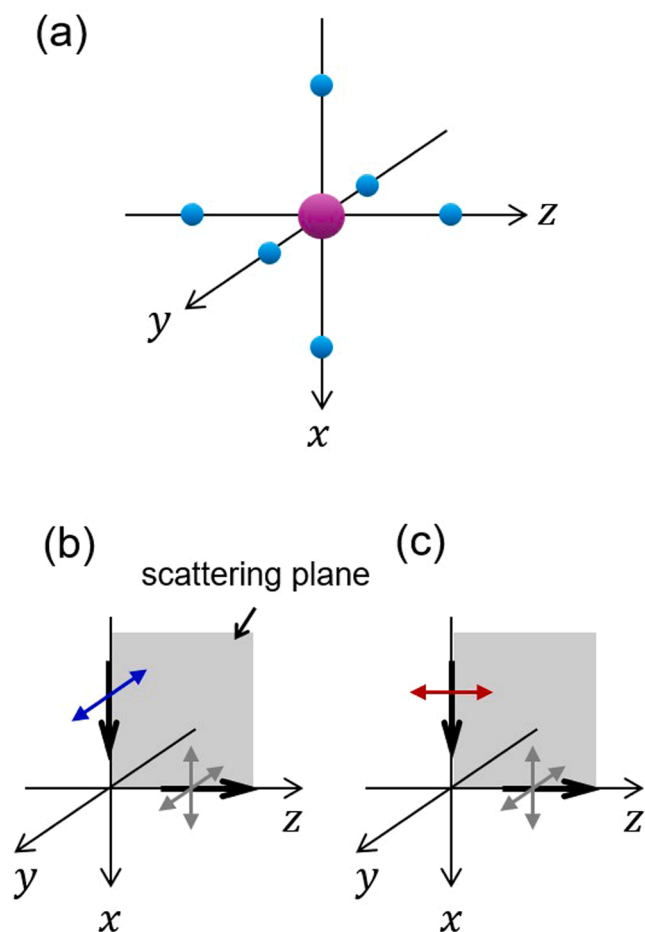


**Fig. 1.** (a) The orthogonal coordinate systems for  $O_h$ . (b), (c) Geometries of the calculations. The scattering plane is the  $xz$ -plane. In the linear vertical (LV) geometry (b), the polarization vector of the incident photon (blue arrow) is perpendicular to the scattering plane. In the linear horizontal (LH) geometry (c), the polarization vector of the incident photon (red arrow) is parallel to the scattering plane.

detail.

Technically, 2p3d-PFY spectroscopy is the (partial) emission energy integrated 2p3d-RIXS spectrum. Utilizing the relationship between 2p3d-PFY and 2p3d-RIXS, one can analyze the 2p3d-PFY spectral structures: a PFY spectrum can be divided into super PFY (sPFY) spectra using partial integrations of signals on a RIXS map. This paper will demonstrate the analyses theoretically and experimentally to reveal the origin of 2p3d-PFY spectral shape differences acquired in LH and LV geometries. As an example, a high-spin  $3d^5$  system in an  $O_h$  point group will be calculated and compared with experimental data in the literature [5]. Then, we will extend the discussion for  $T_d$  symmetry and compare the spectra with experimental data from our original experimental results of wurtzite-AlN films doped with Mn ( $Al_{1-x}Mn_xN$ ). These two point symmetries,  $O_h$  and  $T_d$ , are important point group symmetries [16] and are often applied as approximated point symmetries for lower symmetry point groups, such as  $D_{2d}$  and  $C_{3v}$ , for simplicity.

In this paper, we will also discuss the 2p3s-PFY spectral shape, which uses the  $3s$  shallow core state as the final state. Contrary to the 2p3d-PFY spectra, 2p3s-PFY spectra have often been assumed to have a one-to-one correspondence with true XAS because the 2p3s fluorescence yield does not depend on the specific X-ray absorption final state. However, since 2p3s-PFY spectroscopy is also based on a two-photon process that abides by propagation direction selection rules, 2p3s-PFY spectra also show geometry dependence. We will calculate a geometry dependence of 2p3s-PFY spectra and compare it with the true XAS

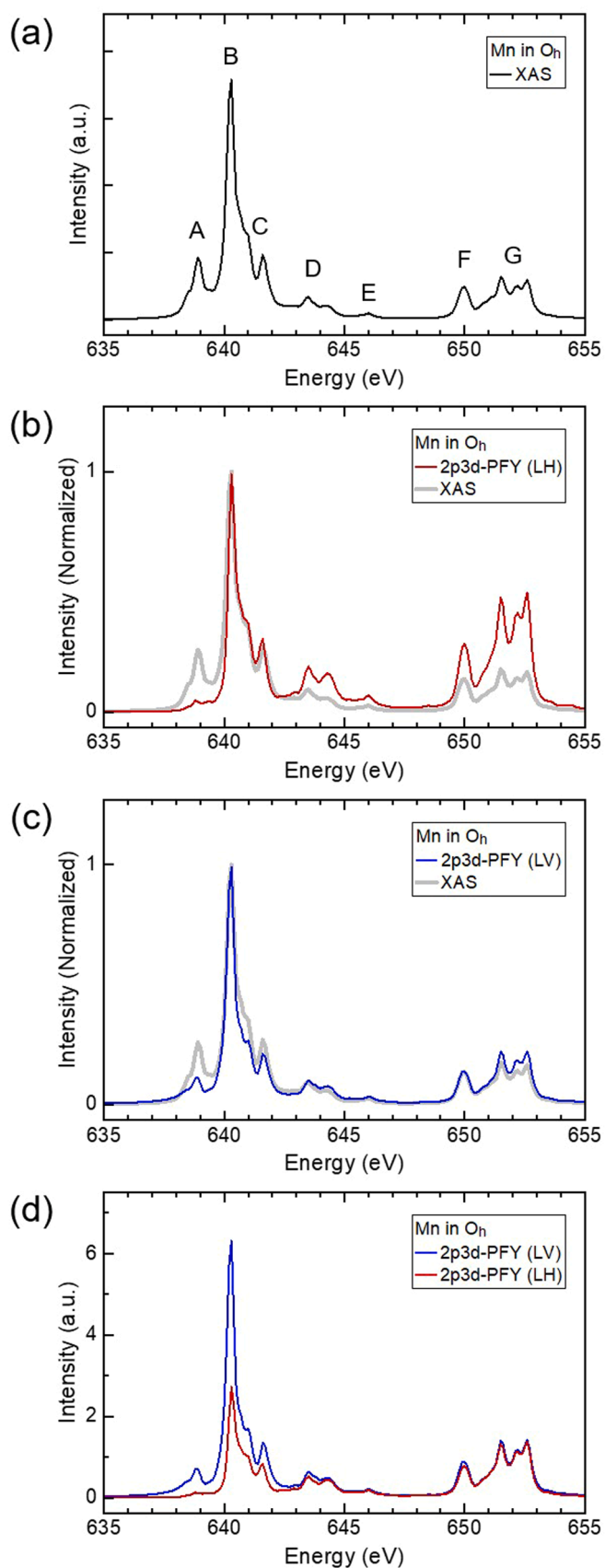


**Fig. 2.** The calculated spectra of high-spin  $3d^5$  Mn in  $O_h$  point symmetry. (a) XAS, (b) 2p3d-PFY in LH geometry with XAS. (c) 2p3d-PFY in LV geometry with XAS. (d) 2p3d-PFY in LH and LV geometries.

## Polarization of emitted light

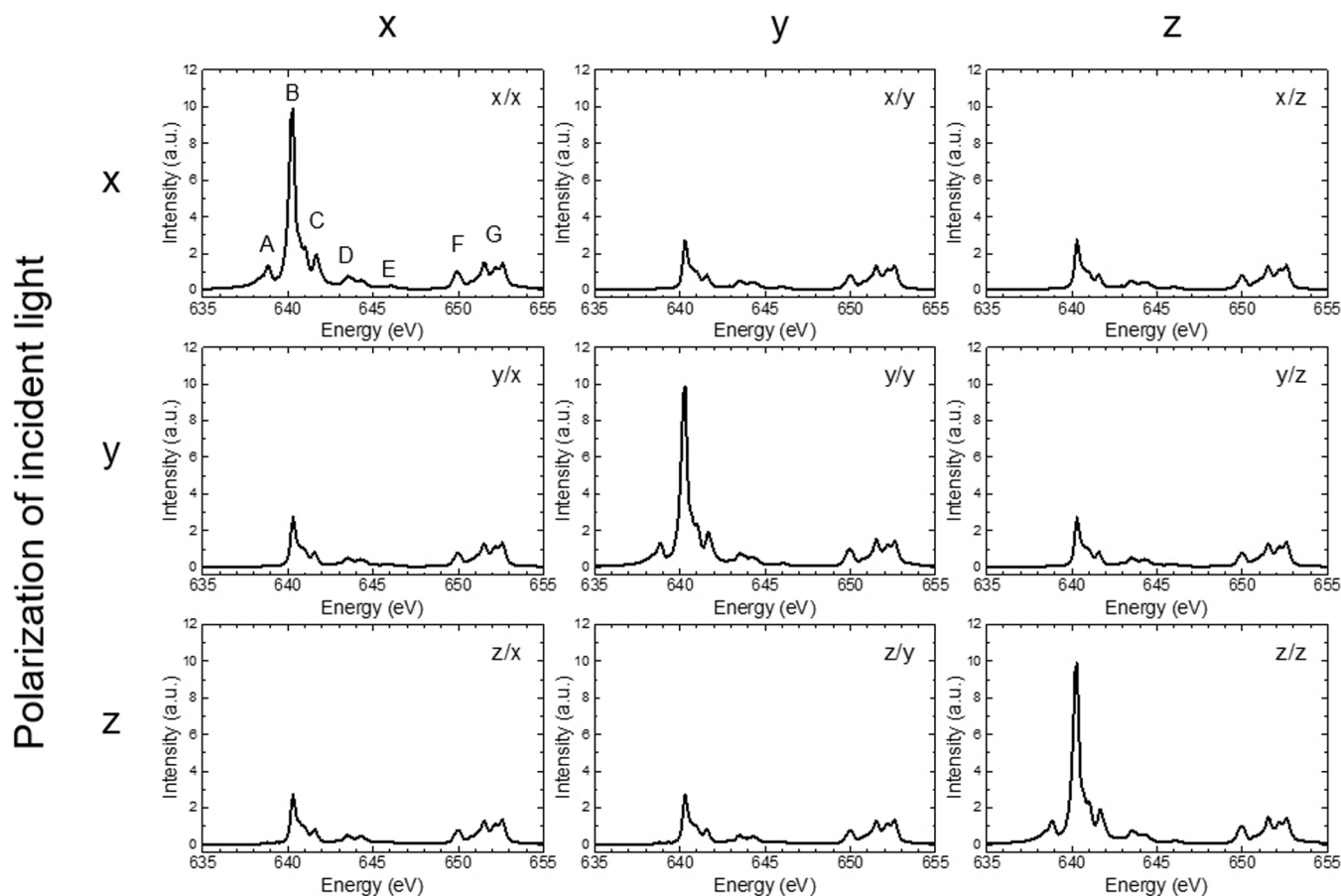


Fig. 3. Calculated 2p3d-PFY spectral matrix for Mn in  $O_h$  symmetry. The element (sub-spectrum)  $y/x$  means that the polarization direction of the incident (absorbed) light is  $y$ , and that of the emitted light is  $x$ .

structures.

## 2. Theoretical and experimental methods

The spectra were calculated using Quanty [17,18] in the crystal field model. For high-spin  $3d^5$  Mn and Fe in octahedral ( $O_h$ ) point group symmetry, atomic Slater integrals were used (scale factor of 0.8 for the Hartree-Fock values). For Mn, a crystal field,  $10Dq$ , value of 1.2 eV was used, the same as the calculation for  $Mn^{2+}$  (aq.) in Ref. [5]. For Fe, a crystal field of 2.0 eV was used to reproduce the PFY spectra of  $Fe^{3+}$  ( $FeCl_3$  in aqueous solution) in Ref. [19]. To easily find structural differences in XAS and PFY spectra, the broadening factors were set to 0.32 eV for Mn and 0.36 eV for Fe (the lifetimes for  $L_{3\alpha}$ ) in full-width half maximum, and no further broadenings were included. For the same reason, the final state broadenings for 2p3d-RIXS were set at 0.05 eV. For simplicity, we put the octahedral ( $MnL_6$  and  $FeL_6$ ,  $L = \text{ligands}$ ,  $O_h$ ) geometry to the orthogonal coordinate system, as depicted in Fig. 1(a). The incident light is linearly polarized and going along the  $x$ -direction. The propagation direction of the emitted light is parallel to the  $z$ -axes for 90-degree scattering. The electric fields of the incident lights are parallel to the  $y$ -axis and the  $z$ -axis for LV and LH geometries, respectively, as shown in Figs. 1(b) and 1(c). Because the polarization of the emitted X-ray cannot be measured, the emission was calculated as combinations of circularly polarized light  $\sigma(x \pm iy)$  to synthesize the spectra. The selection rules for the two-photon process were derived using the

Clebsch-Gordan coefficients following Refs. [9,14,15]. The Clebsch-Gordan coefficient tables are shown in Table S1.

To extend the discussion to a  $T_d$  point symmetry, we chose Mn in wurtzite  $Al_{1-x}Mn_xN$  ( $x = 0.015$  and  $0.043$ , i.e., 1.5 and 4.3 at% in cations, Fig. S1). Except for the importance of the system for various applications such as spintronics [20] and phosphor [21–23], where understanding the electronic structure of Mn is crucial, there are some advantages in the  $Al_{1-x}Mn_xN$  as an experimental case study because it is a dilute system, the FY saturation effect can be avoided, and Mn-Mn interactions can be neglected. Also, there is no need to take care of the dispersion of the energy states. The growth conditions were reported elsewhere [24]. 2p3d-PFY and 2p3d-RIXS spectra were acquired with incident angles to the film surface at  $85^\circ$  (normal incidence), and the scattering angle was  $90^\circ$ . In addition, 2p3d-PFY spectra were acquired with a 45-degree scattering angle for the normal incidence. These experimental configurations are summarized in Table S2. These spectra were obtained at BL27SU [25,26] of SPring-8 in Japan. Theoretical calculations were performed as a high-spin  $3d^5$  Mn in  $T_d$  symmetry. The scale factors for the Hartree-Fock values and  $10Dq$  were chosen as 0.65 and 0.5 eV, respectively, to reproduce the experimental spectra of the  $Al_{1-x}Mn_xN$  film. Because the samples were  $c$ -axis-oriented polycrystalline films [24], we calculated the spectra using the axes that fit the experimental geometries as shown in Fig. S2(a), in addition to the same setting as the case for  $O_h$  in Fig. S2(b).

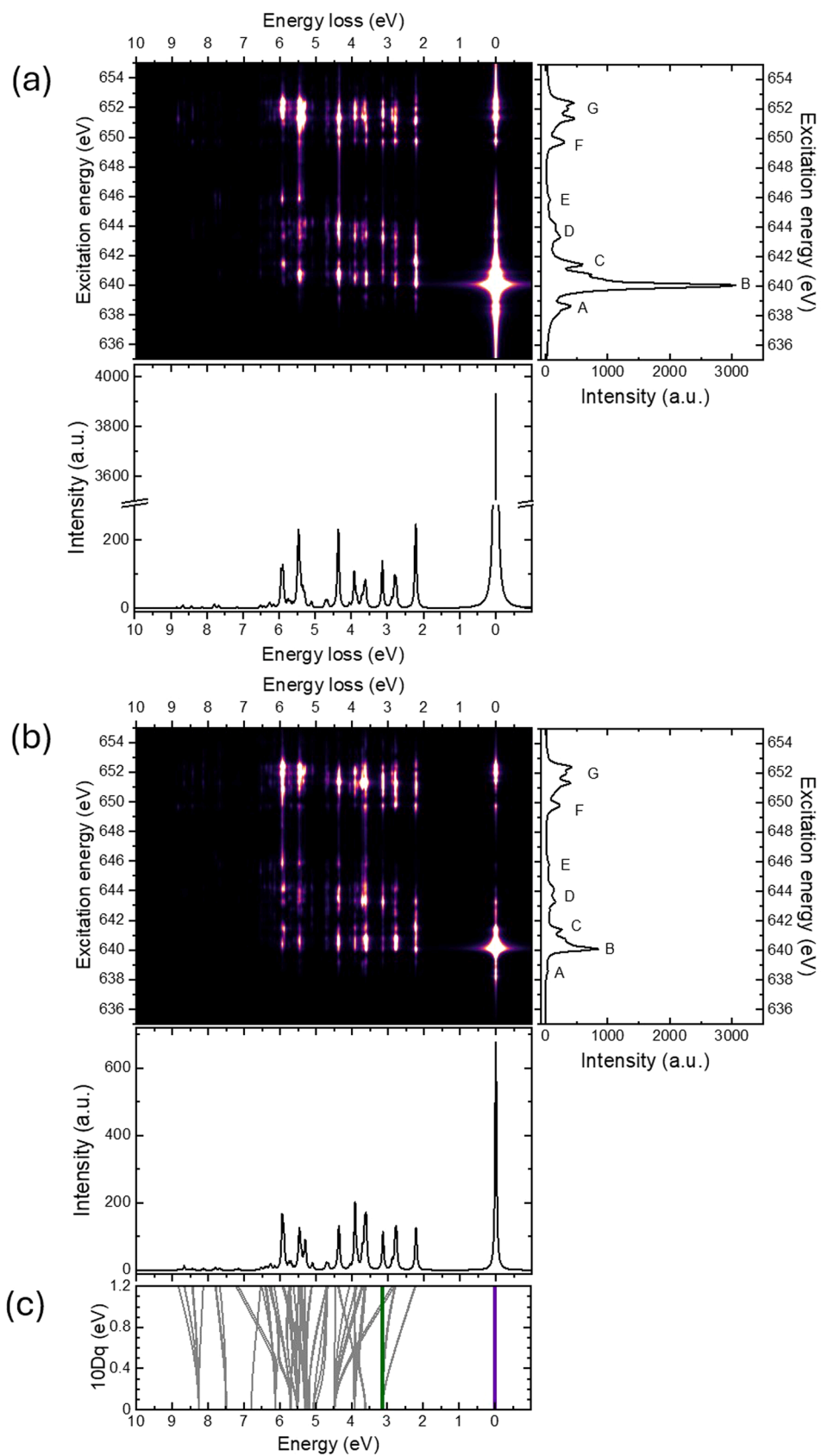


**Fig. 4.** Calculated 2p3d-RIXS maps (excitation vs. energy loss plot); (a) diagonal and (b) off-diagonal sub-maps. The RIXS maps are plotted with the same intensity scale. The right-side spectra are total RIXS yield spectra, which correspond to the 2p3d-PFY sub-spectrum in Fig. 3. The spectra on the RIXS maps are the RIXS spectra integrated over  $L_2$  and  $L_3$  edges. (c) calculated Tanabe-Sugano diagram.

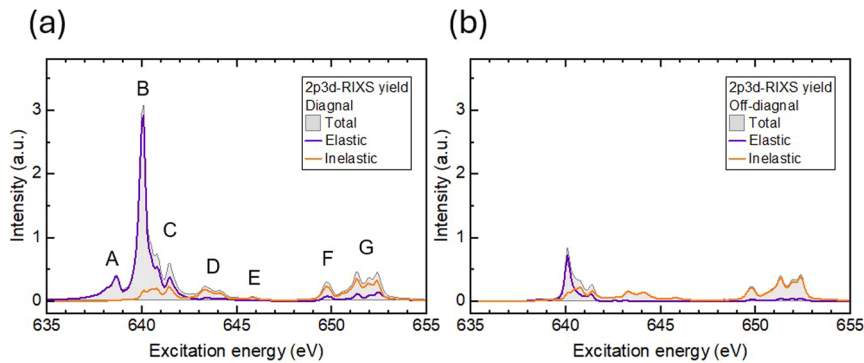


Fig. 5. Calculated 2p3d-RIXS yield from elastic and inelastic regions with a total yield of (a) diagonal and (b) off-diagonal sub-spectra.

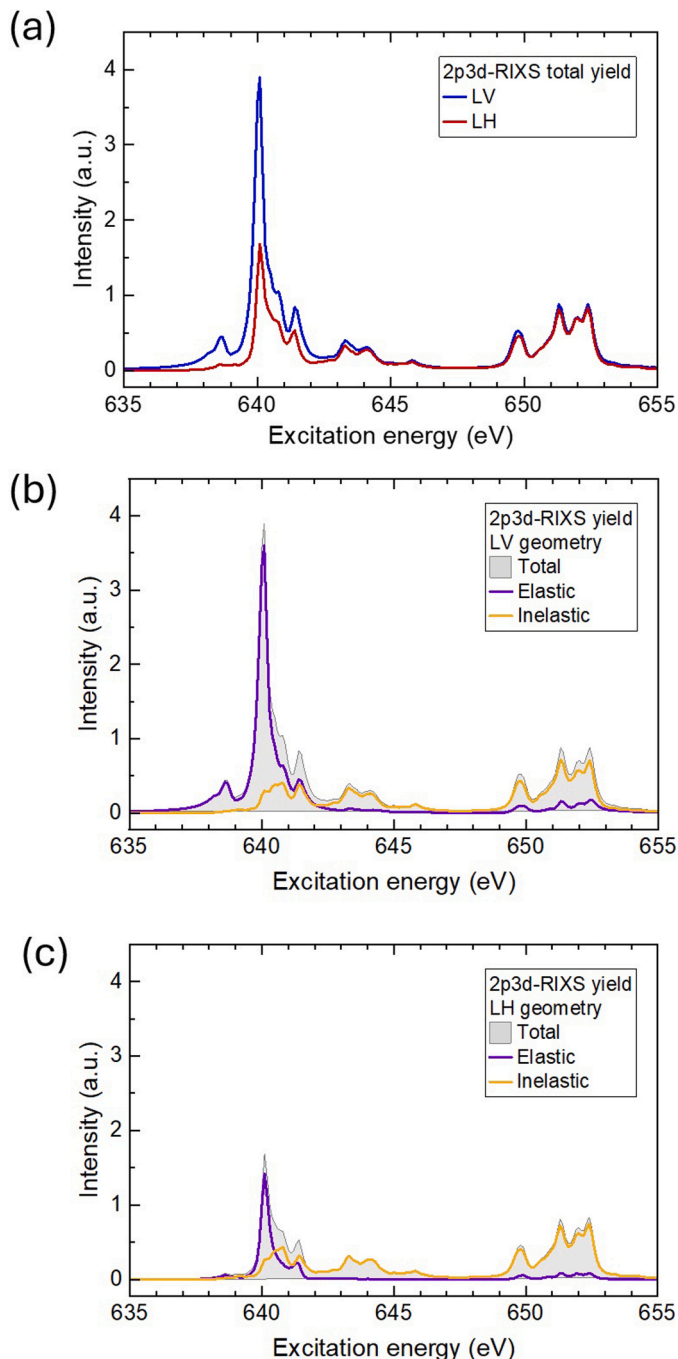


Fig. 6. (a) Calculated 2p3d-RIXS total yield spectra. Calculated 2p3d-RIXS partial yield spectra in (a) LV and (b) LH geometries.

### 3. Results and discussion

#### 3.1. 2p3d-PFY calculations for octahedral symmetry and polarization selection rule

The calculated XAS spectrum for Mn in  $O_h$  symmetry is shown in Fig. 2(a). The peak labels are the same as in Ref. [5]. Fig. 2(b) is the 2p3d-PFY spectrum in LH geometry with the XAS spectrum normalized at peak B, and the tendency reported in Ref. [5] is well reproduced. Fig. 2(c) shows the 2p3d-PFY spectrum in the LV geometry with the XAS spectrum. In the LV geometry, the spectrum shape is closer to the XAS spectrum than the LH geometry; however, there are still differences in the relative intensities. The 2p3d-PFY spectra in the LV and LH geometries are shown in Fig. 2(d). These comparisons with the XAS spectrum remind us that a 2p3d-PFY spectral shape can differ from a true XAS one not only due to a state-dependency in radiation decay but also a measurement geometry, as indicated in Refs. [4,5].

A closer look at the geometry dependence of the 2p3d-PFY spectra in Fig. 2(d) shows that (i) the intensity difference is large in the  $L_3$  region and small in the  $L_2$  region. (ii) The spectrum in the LV geometry presents all the peaks A to G. In contrast, the spectrum in the LH geometry shows vanishingly low intensity of peak A. (iii) The intensities of peaks B and C in the LH geometry are almost half in the LV geometry, while the intensities of peaks D and E are not much different in the two geometries.

To figure out the cause of these geometry dependences, we first derive the selection rules for the two-photon process qualitatively in the LV and LH geometries following the derivation in Refs. [9,14,15] applied for 2p3d-RIXS spectra. A RIXS spectrum is described by the Kramers-Heisenberg formula;

$$F(\Omega, \omega) = \sum_f \left| \sum_m \frac{\langle f | T_e | m \rangle \langle m | T_a | g \rangle}{\Omega + E_g - E_m - i\Gamma_m} \right|^2 \times \delta(\Omega + E_g - \omega - E_f) \quad (1)$$

where  $\Omega$  is the incident photon energy,  $|g\rangle$ ,  $|m\rangle$ , and  $|f\rangle$  are the ground, the intermediate, and the final states of RIXS with the energies  $E_g$ ,  $E_m$ , and  $E_f$ .  $\omega$  is emitted photon energy.  $T_a$  and  $T_e$  are the electric dipole transition operators for the absorption and emission processes, respectively. In the point symmetry  $O_h$ , the representation of the operators is  $T_{1u}$ . To discuss the geometry dependence, one needs to add the basis,  $\gamma$ , of these operators:  $\gamma = \{\alpha, \beta, \gamma\}$  for  $T_{1u}$ . When the quantization axis is  $[001]$ ,  $\gamma$  is  $\{x, y, z\}$  for  $T_1$ . Using the table of Clebsch-Gordan coefficients summarized in Table S1, the selection rules for the  $90^\circ$ -scattering are deduced as follows:

$$LV: \sum_{\gamma=x,y} A_1 \otimes T_{1u,\gamma} \otimes T_{1u,\gamma} = A_1 \oplus E \oplus T_1 \oplus T_2 \quad (2)$$

$$LH: \sum_{\gamma=x,y} A_1 \otimes T_{1u,z} \otimes T_{1u,\gamma} = T_1 \oplus T_2 \quad (3)$$

The selection rules suggest that energy states with irreducible representations  $A_1$  and  $E$  are forbidden as the final states in the LH

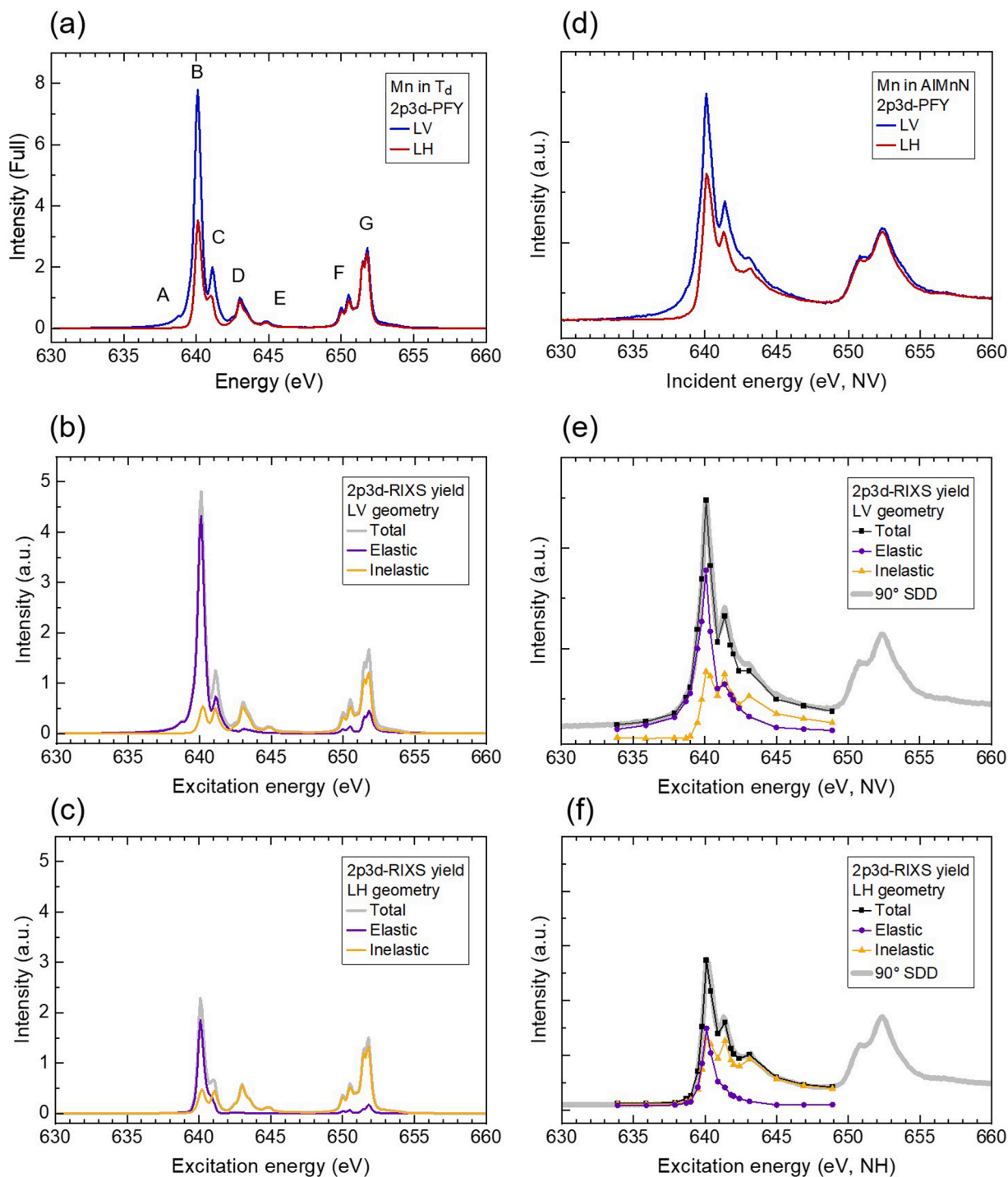


Fig. 7. Calculated 2p3d-PFY and RIXS yield spectra of high-spin  $3d^5$  Mn in  $T_d$ . (d)–(f) depict corresponding experimental spectra of Mn in the  $Al_{1-x}Mn_xN$  ( $x = 0.015$ ) film.

geometry. Thus, the smaller peaks A, B, and C of the 2p3d-PFY spectrum observed in the LH geometry can be due to the lack of contribution of these signals.

### 3.2. 2p3d RIXS and 2p3d PFY from polarization matrices

We have derived the selection rules involving the polarizations of light and propagation directions. Next, we will calculate them quantitatively as spectral elements of a  $3 \times 3$  matrix for polarization vectors set of light,  $\{x, y, z\}$  using the same parameters as the 2p3d-PFY spectra calculations in Fig. 2. Fig. 3 depicts them as the matrix; a diagonal

element is a 2p3d-PFY sub-spectrum in which the incident light's polarization direction is conserved in the emitted light, and an off-diagonal element is non-conserved. The  $y/x$  element means that the polarization direction of the incident (absorbed) light is  $y$ , and that of the emitted light is  $x$ , which corresponds to  $A_1 \otimes T_{1u,y} \otimes T_{1u,x}$ . In the spectral matrix, one can find that signals in the  $L_3$  region are larger in the diagonal sub-spectra than in the off-diagonal ones. Also, the diagonal sub-spectra present peak A, while the off-diagonal ones have almost no intensity in the region of peak A. In addition, the intensities of peaks B and C in the diagonal sub-spectra are much larger than those in the off-diagonal sub-spectra. These results suggest that the difference between the spectra in

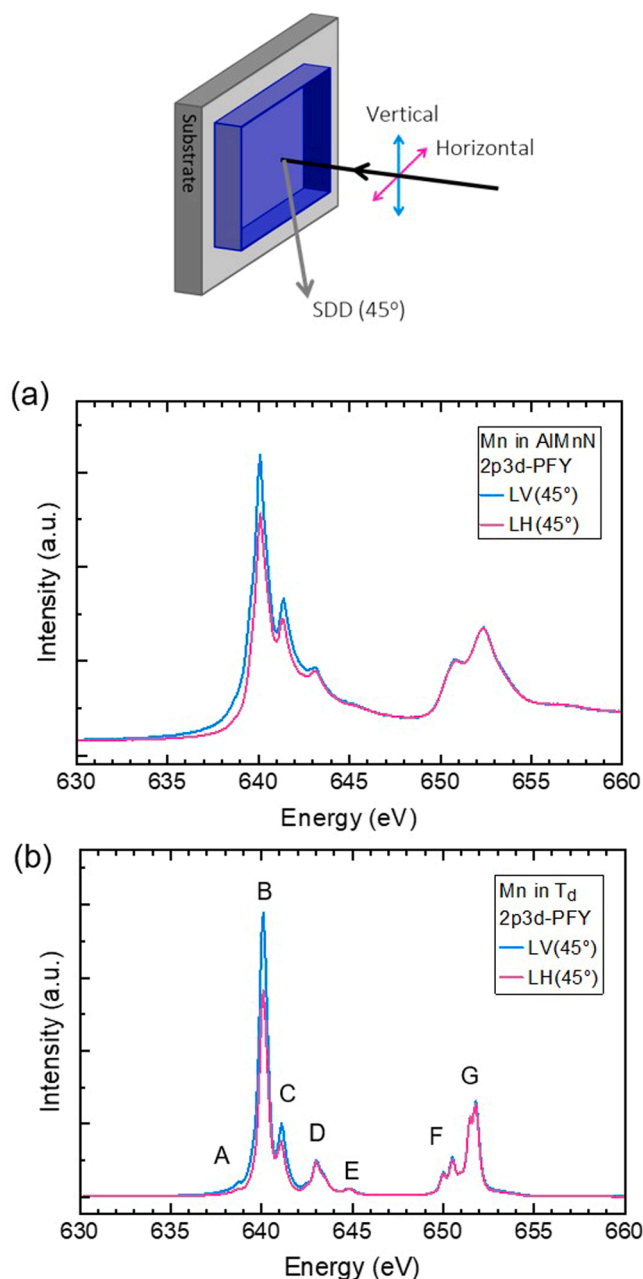


**Fig. 8.** (a) Experimental 2p3d-PFY spectra of Mn in the  $\text{Al}_{1-x}\text{Mn}_x\text{N}$  ( $x = 0.015$ ) film obtained with a scattering angle of 45 degrees. (b) Corresponding theoretical spectra for LV and LH geometries.

the LV and LH geometries in Fig. 2(d) can be traced back essentially to the diagonal (conserved) and off-diagonal (non-conserved) sub-spectra.

To analyze the sub-spectra of 2p3d-PFY, diagonal and off-diagonal 2p3d-RIXS sub-maps were calculated and shown in Figs. 4(a) and 4(b), respectively. These maps are plotted on the same intensity scale. The right-side panels depict the total RIXS yield spectra, corresponding to the 2p3d-PFY sub-spectra in Fig. 3. The RIXS spectra integrated over  $L_2$  and  $L_3$  edge regions are plotted under the maps; the integrated elastic peak height ratio of the off-diagonal to diagonal sub-maps is less than 0.2. On the contrary, the peak heights of inelastic signals in the off-diagonal and diagonal sub-maps are roughly comparable. Fig. 4(c) is a calculated Tanabe-Sugano diagram. The energy levels at  $10Dq = 1.2$  eV correspond to the energy loss of the RIXS peaks. The purple line is the ground state,  ${}^6A_1$ , and the green line is the excited state,  ${}^4E$  plus  ${}^4A_1$ . It suggests that the signal of E, one of the excited states, is considerably

weak comparing the signal of the ground state  $A_1$ , even in the diagonal element, where the multiplet E is allowed along with  $A_1$ . Thus, from a practical (experimental) point of view, it is reasonable to construct partial 2p3d-RIXS yield spectra divided into two regions, elastic and inelastic regions, to analyze the 2p3d-PFY spectra. Fig. 5(a) and 5(b) depict the partial RIXS yield spectra from the elastic and inelastic regions of the diagonal and off-diagonal sub-maps in Figs. 4(a) and 4(b). These results show that peak A is composed of elastic signals. Peak B is mainly from the elastic signals, with small contributions of inelastic signals. At peak C, the elastic signal yield is larger than inelastic in the diagonal sub-spectrum. These findings explain the lack of peak A and small peak B and C in off-diagonal 2p3d-PFY sub-spectra. It is worth noting that these findings imply that one might find the diagonal and off-diagonal sub-spectra themselves if one can acquire 2p3d-PFY and 2p3d-RIXS spectra by resolving the polarization of the emitted light.

The total RIXS yield spectra in the LV and LH geometries by calculating the emitted light as circularly polarized ones  $\sigma(x \pm iy)$  are shown in Fig. 6(a), corresponding to 2p3d-PFY spectra in Fig. 2(d). The partial RIXS yield spectra in the LV and LH geometries are plotted in Figs. 6(b) and 6(c). In conjunction with the selection rules using the Clebsch-Gordan coefficients discussed above, it can be stated that the large deviation of the 2p3d-PFY spectrum in the LH geometry from the true XAS spectrum is due to the lack of elastic signals, in other words, the lack of information on the ground state  $A_1$ . We will discuss later why we still see the elastic signals in the LH geometry, which are predicted as forbidden above with the Clebsch-Gordan coefficient.

### 3.3. 2p3d PFY calculations for tetrahedral symmetry

The same as the high-spin  $3d^5$  system in  $O_h$  symmetry discussed above, some systems have ground state terms that are forbidden in LH geometry; for  $O_h$  symmetry,  $d^0$  ( $A_1$ ),  $d^3$  ( $A_2$ ), high-spin  $d^8$  ( $A_2$ ), and low-spin  $d^6$  ( $A_1$ ). For  $T_d$  symmetry, those are  $d^0$  ( $A_1$ ),  $d^2$  ( $A_2$ ), high-spin  $d^5$  ( $A_1$ ), high-spin  $d^7$  ( $A_2$ ), and low-spin  $d^4$  ( $A_1$ ). A  $T_d$  point symmetry often appears for a 3d-transition metal substituting a cation site in a compound semiconductor. We chose Mn in a wurtzite AlN film for a practical experimental demonstration of 2p3d-PFY spectrum analysis using 2p3d-RIXS partial yield spectra. Fig. 7(a)–(c) depict the theoretical 2p3d-PFY and 2p3d-RIXS yield spectra of high-spin  $3d^5$  Mn in  $T_d$ . The geometry dependence in these theoretical spectra resembles the theoretical spectra for  $3d^5$  in  $O_h$ . Fig. 7(d)–(f) depict corresponding experimental spectra of Mn in the  $\text{Al}_{1-x}\text{Mn}_x\text{N}$  ( $x = 0.015$ ) film. (The experimental and theoretical 2p3d-RIXS spectra are shown in Fig. S3.) It was found that the theoretical 2p3d-PFY spectra reproduced the experimental spectra well, including the geometry dependence. Also, the theoretical geometry dependence of the partial RIXS yield spectra reproduces the experimental ones.

Here, we emphasize that the two selection rules for the electric dipole transition and for the propagation direction are separate. For example, the multiplet term  $A_2$  is one of the excited states of high-spin  $3d^5$  systems in  $O_h$  (and  $T_d$ ) symmetries. However, the state  $A_2$  is electric dipole forbidden; both transition from  $A_1$  to  $A_2$  (absorption) and  $T_1$  to  $A_2$  (emission). Thus, there is no  $A_2$  in Eqs. (2) or (3) as a final state. On the contrary, a transition from  $T_1$  to  $A_1$  is electric dipole allowed; however, propagation of the emitted light is not permitted for an LH geometry in 90 degrees of scattering angle.

To further verify that the geometry dependence of 2p3d-PFY spectra is due to the propagation selection of the emitted light, we measured PFY spectra at scattering angles of 45 degrees. With a scattering angle other than 90 degrees, the selection rules in Eqs. (2) and (3) should be somewhat relaxed, and the difference in the spectral shapes in LH and LV is expected to be small. Figs. 8(a) and 8(b) show the experimental and theoretical spectra. In both the experimental and theoretical spectra of LH(45°), small structures appeared at peak A region, and peaks B and C intensities became stronger, which implies the supposition is accepted. So far, we have tested for Mn in the *c*-axis-oriented wurtzite  $\text{Al}_{1-x}\text{Mn}_x\text{N}$

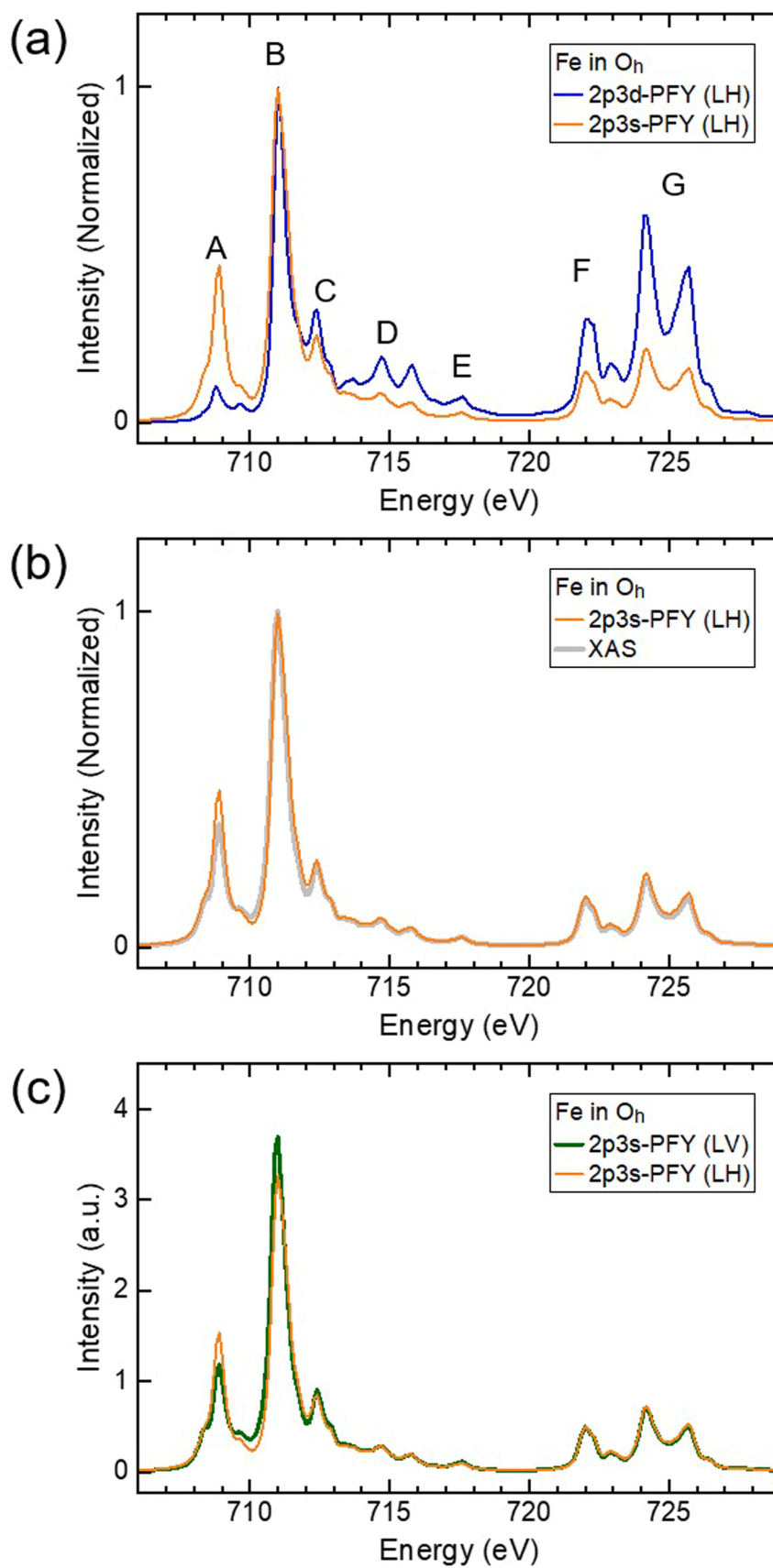


**Fig. 9.** The calculated spectra of high-spin  $3d^5$  Fe in  $O_h$  point symmetry. (a) 2p3d-PFY and 2p3s-PFY in LH geometry. (b) 2p3s-PFY in LH geometry with XAS. (c) 2p3d-PFY in LH and LV geometries.

## Polarization of emitted light

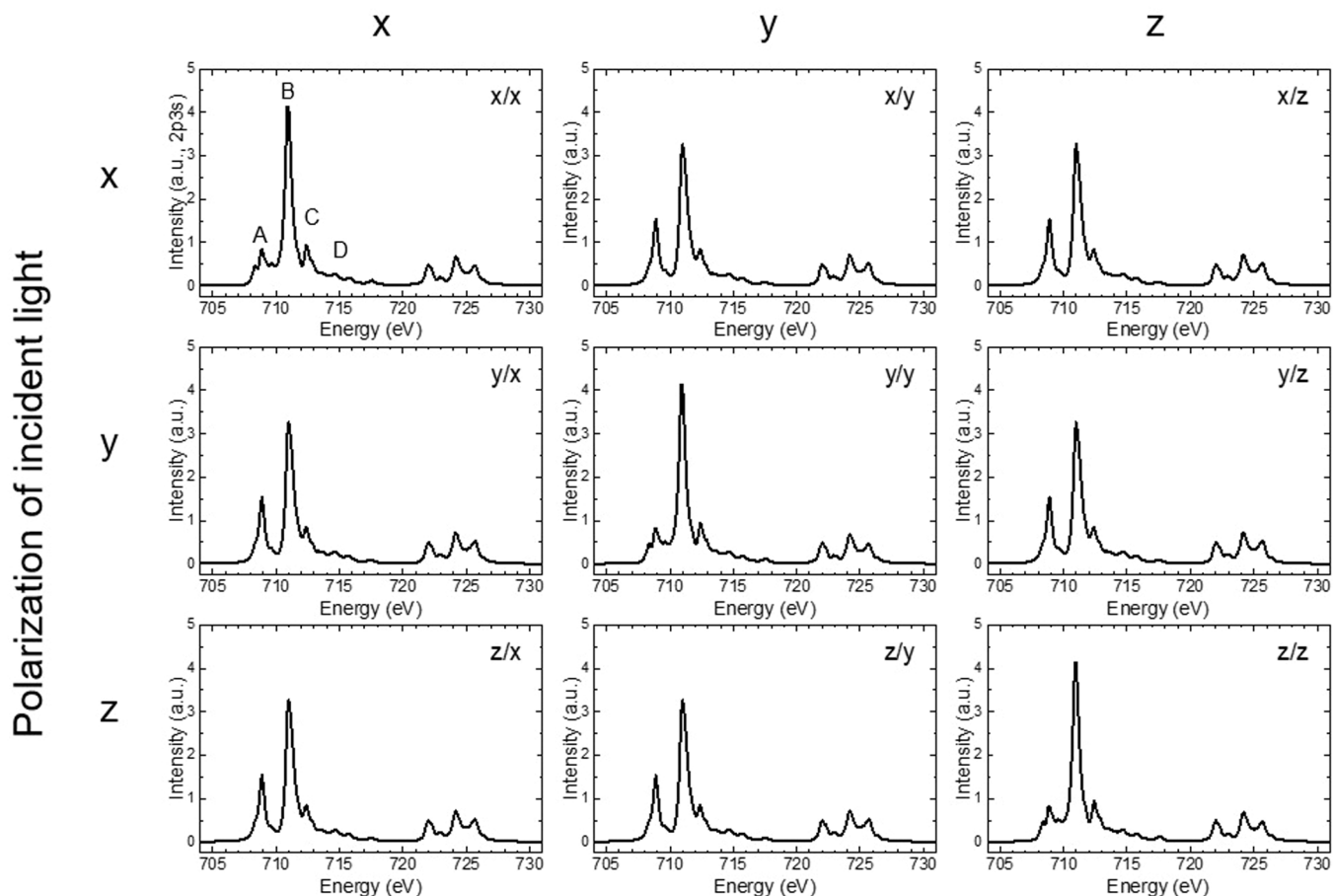


**Fig. 10.** Calculated 2p3s-PFY spectral matrix for Fe in  $O_h$  symmetry. The element (sub-spectrum)  $y/x$  means that the polarization direction of the incident (absorbed) light is  $y$ , and that of the emitted light is  $x$ .

film using the custom axes along with the  $c$ -axis and in the  $c$ -plane to compare the experimental results. To generalize the analyses, we calculated the  $xyz$ -system and found that the polarization dependences also appear for the  $xyz$ -system (Fig. S4).

We propose a candidate mechanism to explain why the LH geometry's elastic signals can be seen in the experimental and theoretical spectra, which are predicted as forbidden in Eqs. (2) and (3). We have discussed the propagation direction rules using the Clebsch-Gordan coefficients tables with monodromy representation, which has the orbital basis. However, the 2p3d-RIXS signals include spin multiplet information; the ground state is the sextet state  ${}^6A_1$ , and the excited states are either quartet  ${}^4E$ ,  ${}^4T_1$ , ... or doublet  ${}^2T_2$ ,  ${}^2E$ , and so on. In this case, the representations have a spin basis and permit a magnetic excitation through spin-orbit couplings. Because the calculations using Quany already include such a spin basis, the RIXS spectra in the LH geometry show elastic signals. Interestingly, the experimental results of Mn in AlMnN presented a smaller intensity of partial RIXS yield from the elastic region in the LH geometry than the calculated one, as shown in Fig. 7. We will discuss such differences and mechanisms in detail in our future paper.

### 3.4. 2p3s PFY calculations

Next, we discuss 2p3s-PFY spectra. Different from 2p3d-PFY spectra, 2p3s-PFY spectra are often assumed to have a one-to-one correspondence with true XAS and have recently gathered interest together with

the inverse PFY spectrum [27]. However, since 2p3s-PFY spectroscopy is also based on a two-photon process, 2p3s-PFY spectra can also show geometry dependence.

Fig. 9(a) is the 2p3s- and 2p3d-PFY spectra in the LH geometry for high-spin  $3d^5$  Fe in  $O_h$  symmetry. (We use the same peak names as the high-spin  $3d^5$  Mn in  $O_h$  in Fig. 2.) Following the procedure described in Ref. [19], the spectra are normalized at peak B. Our calculated 2p3s- and 2p3d-PFY spectra reproduce well the experimental ones of  $FeCl_3$  aqueous solution and theoretical spectra for  $[Fe(H_2O)_6]^{3+}$  in Ref. [19]. Fig. 9(b) compares the 2p3s-PFY spectrum in LH geometry with the XAS spectrum. The 2p3s-PFY spectrum in LH geometry shows a very close shape with the XAS spectrum in the entire region of  $L_2$  and  $L_3$ . However, as shown in Fig. 9(c), the 2p3s-PFY spectra show small but obvious geometry dependence: larger peak A and smaller peak B in the LH geometry than those in the LV geometry. The ground state of the high-spin  $3d^5$  Fe in  $O_h$  is  ${}^6A_1$ , so the same propagation direction selections, Eqs. (2) and (3) should be applied. Fig. 10 shows a calculated 2p3s-PFY spectral matrix for Fe in  $O_h$  point group symmetry. The diagonal sub-spectra show larger peak B than the off-diagonal ones, the same as the case of 2p3d-PFY of Mn in  $O_h$  in Fig. 3. On the contrary, the peak height of peak A is smaller in the diagonal sub-spectra than in the off-diagonal ones. Unlike the 2p3d case, the final states of 2p3s-PFY spectroscopy have a core hole in a 3s orbital ( $3s^1 3d^{n+1}$ ), which makes interpreting this tendency not straightforward. However, it is worth noting that a 2p3s-PFY integrated in all directions (the sum of all sub-spectra in Fig. 10) forms a spectrum that perfectly coincides with the true XAS spectrum (Fig. 11

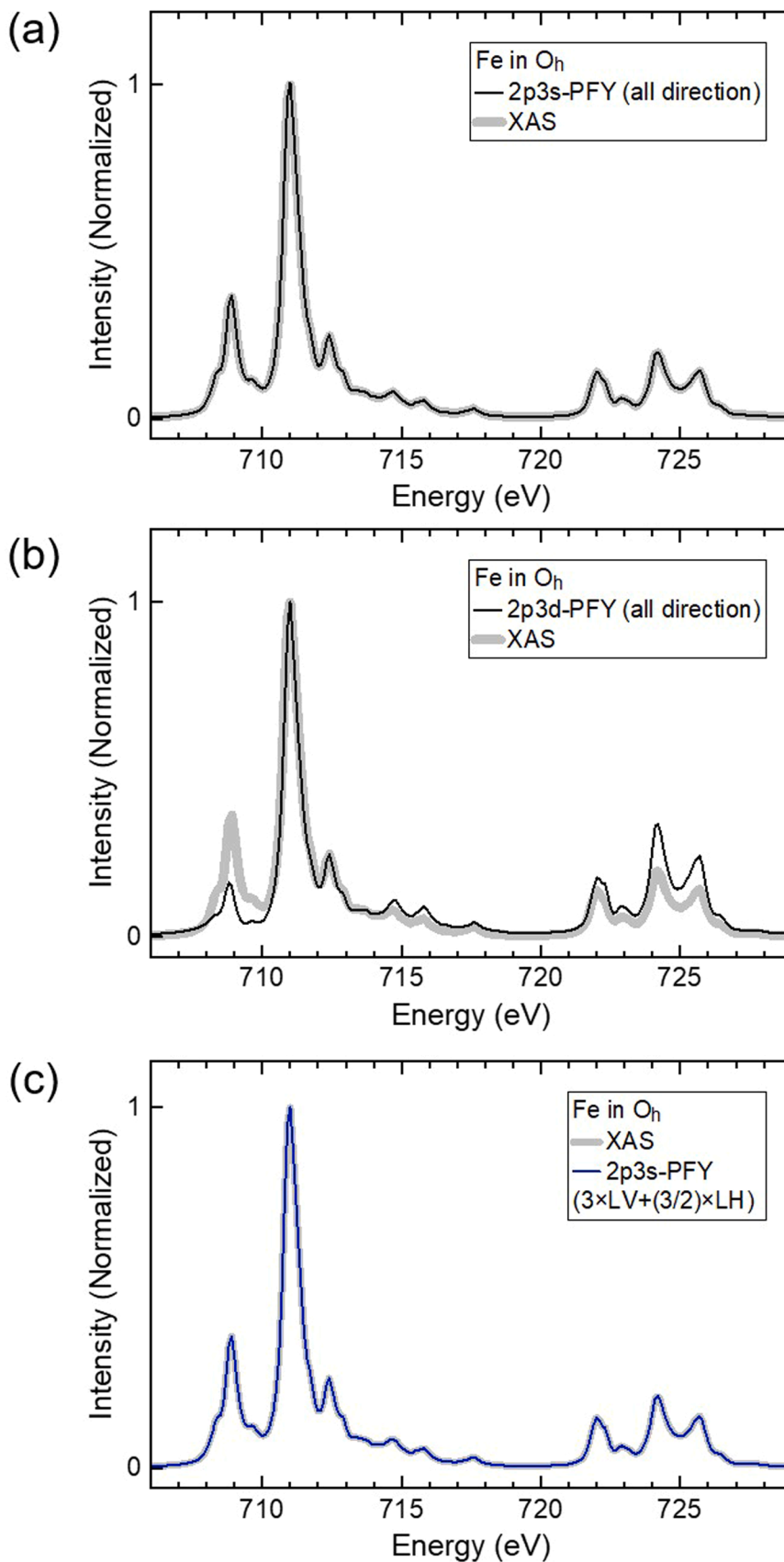


**Fig. 11.** The calculated spectra of Fe in  $O_h$  point symmetry. (a) 2p3s-PFY and (b) 2p3d-PFY integrated in all directions compared with XAS. (c) Calculated combination of 2p3s-PFY spectra in LV and LH geometries for Fe in  $O_h$  symmetry with true XAS spectrum.

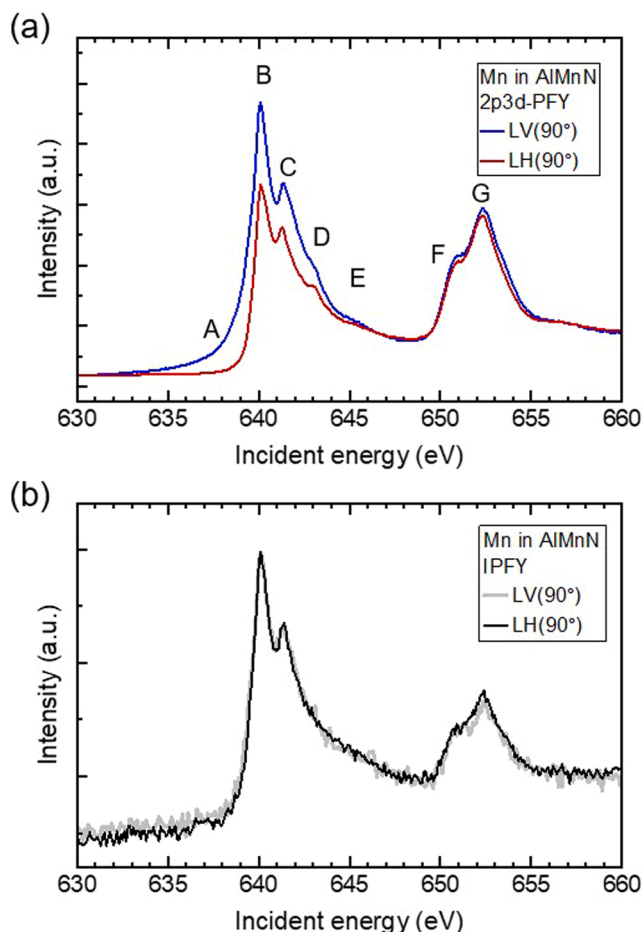


Fig. 12. 2p3d-PFY (a) and inversion PFY (b) spectra of Mn in an  $\text{Al}_{1-x}\text{Mn}_x\text{N}$  ( $x = 0.043$ ) film. The scattering angle was 90 degrees.

(a), while a 2p3d-PFY shows a different spectrum shape (Fig. 11(b)). The former is a consequence that 3s-2p emissions do not depend on  $2p^5 3d^{n+1}$  states, and the latter is that 3d-2p emissions depend on the  $2p^5 3d^{n+1}$  states.

An interesting finding in the 2p3s-PFY spectroscopy is that one can obtain true XAS structure experimentally by combining the 2p3s-PFY spectra in the LV and LH geometries, as shown in Fig. 11(c). The 2p3s-PFY spectra in the LV and LH geometries are obtained as the sum of  $y/r$  and  $y/l$  components and that of  $z/r$  and  $z/l$ , respectively, as shown in Fig.S5. As  $y/r$  ( $= y/l$ ) sub-spectrum coincides with the combination of  $y/x$  and  $y/y$  (1 off-diagonal and 1 diagonal in Fig. 10). Also,  $z/r$  ( $= z/l$ ) sub-spectrum is the combination of  $z/x$  and  $z/y$  (2 off-diagonal in Fig. 10). Thus, the true XAS shape, the sum of 3 diagonal plus 6 off-diagonal sub-spectra, is obtained by combining 3 LV and 3/2 LH spectra of 2p3s-PFY as shown in Fig. 11(c). A 2p3s-PFY integrated in all directions (Fig. 11(a)) also gives the true XAS structure. However, a combination of LV and LH spectra is more realistic from an experimental point of view.

#### 4. Conclusions

For a 2p3d-PFY spectrum of a high-spin  $3d^5$  transition metal in Oh and Td symmetries, the origin of the distorted structures from the true XAS spectrum was explained from the propagation direction selection rule. At the same time, we offer a way to analyze a 2p3d-PFY spectrum structure using partial integrations of RIXS signals. In principle, one can make a 2p3d-RIXS partial yield spectrum for any region of interest from a 2p3d-RIXS map. As the final states of 2p3d-fluorescence and RIXS have no core hole, a 2p3d-PFY spectrum can be reduced to multiplets in the

energy levels in the Tanabe-Sugano diagram.

More simply, we offer the usage of 2p3d-PFY spectra to find a buried peak in a true XAS spectrum. Figs. 12(a) and 12(b) show 2p3d-PFY and inversion PFY (IPFY, N 1s2p emission) spectra of Mn in an  $\text{Al}_{1-x}\text{Mn}_x\text{N}$  ( $x = 0.043$ ) film. The IPFY spectra, thought to correspond to the true XAS spectra, showed fewer structures than the 2p3d-PFY spectra. It means that one can find an almost buried peak (for example, peak D in the 2p3d-PFY spectra) by suppressing the strong elastic signal detection using the LH geometry by taking advantage of a two-photon process in the 2p3d-PFY method. Finding such buried peaks can be crucial to deriving important electronic structure parameters. Our attempts would shed light on the usage of 2p3d-PFY spectra, which are distorted from true XAS spectra but easy to obtain for various materials.

We also discussed the geometry dependence of 2p3s-PFY spectra of high-spin  $3d^5$  in Oh symmetry. Reflecting that a 2p3s-PFY is also a two-photon process, the theoretical 2p3s-PFY spectra showed geometry dependence. We offer a way to obtain a true XAS structure using a combination of 2p3s-PFY spectra obtained in LV and LH geometry.

#### CRediT authorship contribution statement

**de Groot Frank M.F.:** Writing – review & editing, Validation, Methodology, Formal analysis, Conceptualization. **Imada Saki:** Writing – original draft, Methodology, Investigation, Funding acquisition, Formal analysis, Data curation, Conceptualization.

#### Declaration of Competing Interest

The authors declare that they have no known competing financial interests or personal relationships that could have appeared to influence the work reported in this paper.

#### Acknowledgments

The synchrotron experiments were performed at the BL27SU, SPring-8, Japan under proposal numbers 2021A1301/1289, 2021B1536, 2022A1149/1150. We are grateful for the help of the beamline staff to set up the experiments. A part of this work was supported by JSPS KAKENHI Grant no. JP24K08077. We thank Drs. Y. Tamenori, L. Duda, S. Butorin, P. Wernet, J-R. Rubensson and A. Hariki for helpful discussions.

#### Appendix A. Supporting information

Supplementary data associated with this article can be found in the online version at [doi:10.1016/j.elspec.2025.147538](https://doi.org/10.1016/j.elspec.2025.147538).

#### Data availability

Data will be made available on request.

#### References

- [1] F.M.F. de Groot, et al., 2p X-ray absorption spectroscopy of 3d transition metal systems, *J. Electron Spectrosc. Relat. Phenom.* 249 (2021) 147061.
- [2] F.M.F. de Groot, M.A. Arrio, P. Saintavit, C. Cartier, C.T. Chen, Fluorescence yield detection: why it does not measure the x-ray absorption cross section, *Solid State Commun.* 92 (1994) 991.
- [3] F.De Groot, Multiplet effects in x-ray spectroscopy, *Coord. Chem. Rev.* 249 (2005) 31.
- [4] R. Kurian, K. Kunnus, P. Wernet, S.M. Butorin, P. Glatzel, F.M.F. de Groot, Intrinsic deviations in fluorescence yield detected x-ray absorption spectroscopy: the case of the transition metal L 2,3 edges, *J. Phys. Condens. Matter* 24 (2012) 452201.
- [5] R. Mitzner, et al., L-edge x-ray absorption spectroscopy of dilute systems relevant to metalloproteins using an x-ray free-electron laser, *J. Phys. Chem. Lett.* 4 (2013) 3641.
- [6] P.S. Miedema, P. Wernet, A. Föhlisch, State-dependent fluorescence yields through the core-valence coulomb exchange parameter, *Phys. Rev. A - At. Mol. Opt. Phys.* 89 (2014).

- [7] F.M.F. de Groot, M.W. Haverkort, H. Elnaggar, A. Juhin, K.-J. Zhou, P. Glatzel, Resonant inelastic x-ray scattering, *Nat. Rev. Methods Prim.* 4 (2024) 45.
- [8] A.W. Hahn, B.E. Van Kuiken, M. Al Samarai, M. Atanasov, T. Weyhermüller, Y. T. Cui, J. Miyawaki, Y. Harada, A. Nicolaou, S. DeBeer, Measurement of the ligand field spectra of ferrous and ferric iron chlorides using 2p3d RIXS, *Inorg. Chem.* 56 (2017) 8203.
- [9] M.O.J.Y. Hunault, Y. Harada, J. Miyawaki, J. Wang, A. Meijerink, F.M.F. De Groot, M.M. Van Schooneveld, Direct observation of Cr<sup>3+</sup> + 3d states in ruby: toward experimental mechanistic evidence of metal chemistry, *J. Phys. Chem. A* 122 (2018) 4399.
- [10] L.J.P. Ament, M. van Veenendaal, T.P. Devereaux, J.P. Hill, J. van den Brink, Resonant inelastic x-ray scattering studies of elementary excitations, *Rev. Mod. Phys.* 83 (2011) 705.
- [11] L. Braicovich, High resolution resonant inelastic x-ray scattering from solids in the soft range, in: *Synchrotron Light Sources and Free-Electron Lasers*, Springer International Publishing, Cham, 2020, pp. 2289–2314.
- [12] F.M.F. de Groot, P. Kuiper, G.A. Sawatzky, Local spin-flip spectral distribution obtained by resonant x-ray raman scattering, *Phys. Rev. B* 57 (1998) 14584.
- [13] S. Sugano, Y. Tanabe, H. Kamimura, *Multiplets of Transition-Metal Ions in Crystals*, 33, Academic Press, 1970.
- [14] M. Matsubara, T. Uozumi, A. Kotani, Y. Harada, S. Shin, Polarization dependence of resonant x-ray emission spectra in early transition metal compounds, *J. Phys. Soc. Jpn.* 69 (2000) 1558.
- [15] M. Matsubara, T. Uozumi, A. Kotani, Y. Harada, S. Shin, Polarization dependence of resonant x-ray emission spectra in 3d transition metal compounds with n = 0, 1, 2, 3, *J. Phys. Soc. Jpn.* 71 (2002) 347.
- [16] G. van der Laan, I.W. Kirkman, The 2p Absorption Spectra of 3d Transition Metal Compounds in Tetrahedral and Octahedral Symmetry, *J. Phys.: Condens. Matter* 4 (1992) 4189.
- [17] M.W. Haverkort, M. Zwierzycki, O.K. Andersen, Multiplet ligand-field theory using Wannier orbitals, *Phys. Rev. B* 85 (2012) 165113.
- [18] M.W. Haverkort, Quanta for core level spectroscopy – excitons, resonances and band excitations in time and frequency domain, *J. Phys. Conf. Ser.* 712 (2016) 012001.
- [19] R. Golnak, J. Xiao, K. Atak, I. Unger, R. Seidel, B. Winter, E.F. Aziz, Undistorted X-ray absorption spectroscopy using s-core-orbital emissions, *J. Phys. Chem. A* 120 (2016) 2808.
- [20] S.J. Pearton, C.R. Abernathy, F. Ren, Nitride-based spintronics, in: *Gallium Nitride Processing for Electronics, Sensors and Spintronics*, Springer London, London, 2006, pp. 261–311.
- [21] M. Mansoor, et al., Optical centers in Cr-, Mn-, and O-doped AlN and their thermodynamic stability designed by a multiscale computational approach, *ACS Appl. Mater. Interfaces* 16 (2024) 69529.
- [22] J. Xu, N.J. Cherepy, J. Ueda, S. Tanabe, Red persistent luminescence in rare earth-free AlN:Mn<sup>2+</sup> phosphor, *Mater. Lett.* 206 (2017) 175.
- [23] N.J. Cherepy, et al., Red-emitting manganese-doped aluminum nitride phosphor, *Opt. Mater.* 54 (2016) 14.
- [24] N. Tatemizo, S. Imada, Y. Miura, K. Nishio, T. Isshiki, Chemical trend in band structure of 3d-transition-metal-doped AlN films, *Mater. Sci. Forum* 924 (2018) 322.
- [25] Y. Tamenori, M. Morita, T. Nakamura, Two-dimensional approach to fluorescence yield XANES measurement using a silicon drift detector, *J. Synchrotron Radiat.* 18 (2011) 747.
- [26] T. Tokushima, Y. Harada, H. Ohashi, Y. Senba, S. Shin, High performance slit-less spectrometer for soft x-ray emission spectroscopy, *Rev. Sci. Instrum.* 77 (2006) 1.
- [27] A.J. Achkar, T.Z. Regier, H. Wadati, Y.-J. Kim, H. Zhang, D.G. Hawthorn, Bulk sensitive x-ray absorption spectroscopy free of self-absorption effects, *Phys. Rev. B* 83 (2011) 081106.